Research Article

Image Processing-Based Recognition of Wall Defects Using Machine Learning Approaches and Steerable Filters

Nhat-Duc Hoang (iD)

Lecturer, Faculty of Civil Engineering, Institute of Research and Development, Duy Tan University, P809-03 Quang Trung, Da Nang, Vietnam

Correspondence should be addressed to Nhat-Duc Hoang; hoangnhatduc@dtu.edu.vn

Detection of defects including cracks and spalls on wall surface in high-rise buildings is a crucial task of buildings' maintenance. If left undetected and untreated, these defects can significantly affect the structural integrity and the aesthetic aspect of buildings. Timely and cost-effective methods of building condition survey are of practicing need for the building owners and maintenance agencies to replace the time- and labor-consuming approach of manual survey. This study constructs an image processing approach for periodically evaluating the condition of wall structures. Image processing algorithms of steerable filters and projection integrals are employed to extract useful features from digital images. The newly developed model relies on the Support vector machine and least squares support vector machine to generalize the classification boundaries that categorize conditions of wall into five labels: longitudinal crack, transverse crack, diagonal crack, spall damage, and intact wall. A data set consisting of 500 image samples has been collected to train and test the machine learning based classifiers. Experimental results point out that the proposed model that combines the image processing and machine learning algorithms can achieve a good classification performance with a classification accuracy rate = 85.33%. Therefore, the newly developed method can be a promising alternative to assist maintenance agencies in periodic building surveys.

1. Introduction

During the construction and maintenance of high-rise buildings, it is very crucial to attain good surface quality of structures due to safety and esthetics aspects. Because of the combined effects of aging, weather conditions, and human activities, the condition of building structures deteriorates over time [1]. If left untreated, damages such as cracks and spalls obviously cause inconvenience for the building's occupants, deteriorate the structural integrity, and lead to a significant reduction of the value of the poorly maintained asset. Therefore, identifying defective areas that appear on surface structure is one of the main tasks in periodic survey buildings.

In high-rise buildings, the components that have large surface areas typically include walls (both concrete walls and brick walls covered by mortar) and slabs. The assessment of concrete slabs is usually performed during the construction phase. It is because during the operation phase, the surface of slab structure is concealed by floor coverings such as ceramic or stone tiles. Therefore, this study focuses on the visual assessment of wall structures.

In Vietnam, periodic surveys on building condition are usually performed by visual assessment of human inspectors. This fact is also common in other countries because visual changes in structures can directly point out the potential problems of building structures [2]. For instances, cracks can be indicators of structural problems including building settlement and degradation of building materials; particularly for concrete walls, spalls can be caused by the corrosion of embedded reinforcement bars [3–5].

In the current practice of building condition assessment, the damages on the surface of building structures are usually inspected by qualified technicians. These technicians often utilize contact-type equipment including profilometer and

measuring tape for identifying the defective areas [6]. Although the manual procedure can help to obtain accurate condition of the structure, it also has several disadvantages. First, the surveying process is strongly affected by the knowledge, experience, and subjective judgment of human inspectors; therefore, this issue can lead to inconsistency of the assessment outcome. Second, the process of visual assessment, measurement, data processing, and report can be very time consuming especially for high-rise buildings with large surface areas needed to be inspected periodically.

Accordingly, it is immensely beneficial for the building owners and maintenance agencies if the manual inspection process can be replaced by a more productive and consistent method of surveying [7]. Among automated methods for building condition evaluation, machine vision based approaches are widely employed due to their ease of access to equipment, their fast computing processes, and the rapid advancements of image processing techniques [8–14].

Hutchinson and Chen [15] presented a statistical-based method for evaluating concrete damage including cracks and spalls and relied on a Bayesian method for recognizing cracks automatically from images. Chen et al. [16] employed the first derivative of a Gaussian filter to analyze multi-temporal images for measuring cracks. Zhu [17] put forward an intelligent method using three circular filters to detect air pockets appearing on the surfaces of concrete.

The level set method and morphological algorithms for image processing have been used by Chen and Hutchinson [18] to identify and analyze cracks in laboratory environment. Lee et al. [19] proposed a model that integrates various image processing operations (brightness adjustment, binarisation, and shape analysis) to facilitate the accuracy of crack detection; in addition, a neural network-based model was implemented to classify crack patterns of cracks. Valença et al. [20] introduced a method based on multispectral image analysis to evaluate and delineate defective areas.

An image processing-based approach for detecting bugholes on concrete surface has been established by Liu and Yang [21]; the employed techniques are contrast enhancement and Otsu thresholding. Kim et al. [22] compared different image binarisation algorithms for identifying cracks in concrete structures. Hoang [23] employed the Otsu method and a gray intensity modification approach for binarizing images and isolating cracks.

Silva and Lucena [24] demonstrated the capability of deep learning approach for concrete crack detection. Dorafshan et al. [25] has recently compared the performances of deep convolutional neural networks and edge detection methods for the task of recognizing concrete cracks. The notable advantage of deep learning approaches is that their feature extraction operators are autonomously constructed during the model training phase [26]. However, methods based on deep learning often necessitate a considerable amount of training samples and require a large computational cost.

As can be seen from the existing literature, most of the previous works have dedicated in constructing models for the classification of crack and noncrack conditions. Few studies have constructed an integrated image processing model for detect cracks and spalls. The objective of the current study is to combine image processing techniques and advanced machine learning algorithms into an integrated model that is capable of detecting and categorizing the defective areas on wall structures. By using an intelligent model that can recognize and categorize types of cracks and spalling areas simultaneously, the task of periodic building condition survey can be executed in a more effective manner.

The feature extraction phase of the new model relies on image processing algorithms of steerable filters and projection integrals. It is because these two algorithms of image processing have demonstrated their usefulness in recognizing defects in pavements [27, 28]. Based on the extracted features, machine learning algorithms including support vector machine (SVM) and least squares support vector machine (LSSVM) are employed to classify input images into five labels: longitudinal cracks, transverse cracks, diagonal cracks, spalls, and intact walls. The reason for the selection of these machine learning approaches is that their outstanding performances in classification tasks have been reported in the literature [29–33].

Based on the aforementioned features, the main contributions of the newly constructed model can be summarized as follows:

(i) Multiple types of cracks (longitudinal cracks, transverse cracks, diagonal cracks) existing in wall structures can be detected and categorized in an integrated model. This can be considered to be a significant improvement since most of the existing models can only produce the prediction outcome of crack or noncrack conditions [13, 23–25].

(ii) Although projection integrals have been utilized in structural defect classification [27, 28], diagonal projection integrals which have been rarely exploited in concrete surface crack categorization are employed in this study to specifically deal with diagonal cracks.

(iii) Cracks and spall damages can be recognized simultaneously in an integrated model which has also rarely been achieved in the current literature.

(iv) Neural networks have been extensively used in concrete crack categorization [19, 34, 35]. However, the applications of SVM and LSSVM in this task are still limited and a comparative work needs to be performed to evaluate the potential of these two advance machine learning algorithms in dealing with the problem of wall defect recognition.

The rest of the paper is organized as follows: the research methodology is reviewed briefly in the next section, followed by the description of the newly constructed automatic approach for wall defect detection; the fourth section reports experimental results of this study, followed by the conclusion in the final section.

2. Research Methodology

2.1. Image Processing Approaches

2.1.1. Steerable Filter (SF). SF [36] is an orientation-selective convolution kernel used widely used for feature extraction. In image processing field, oriented filters are often employed in various vision and image processing tasks including edge detection and texture analysis [37]. Since cracks and spalls on wall surface have distinctive edges and patterns; the utilization of SF can be helpful to recognize these defects.

SF is based on the computation of directional derivatives of Gaussians; accordingly, these filters can be used to construct local orientation maps of a digital image [37]. SF is essentially a linear combination of Gaussian second derivatives. For an image $I(x,y)$, a 2-D Gaussian at a certain pixel is computed in the following formula [38]:

$$G(x, y, r) = \frac{1}{\sqrt{2\pi}r} \exp \frac{-(x^2 + y^2)}{2r^2}, \tag{1}$$

where r is a free parameter which denotes the Gaussian function variance.

The expression of the SF formulation with an orientation of θ is given as follows:

$$F(x, y, r, \theta) = G_{xx} \cos^2(\theta) + 2G_{xy} \cos(\theta)\sin(\theta) + G_{yy} \sin^2(\theta), \tag{2}$$

where G_{xx}, G_{xy}, and G_{yy} denote the Gaussian second derivatives and their expression are given in the following equations:

$$G_{xx}(x, y, r) = \frac{(x^2 - r^2)\exp(-(x^2 + y^2)/2r^2)}{\sqrt{2\pi}r^5},$$

$$G_{yy}(x, y, r) = \frac{(y^2 - r^2)\exp(-(x^2 + y^2)/2r^2)}{\sqrt{2\pi}r^5},$$

$$G_{xy}(x, y, r) = G_{xy}(x, y, r) = \frac{xy \exp(-(x^2 + y^2)/2r^2)}{\sqrt{2\pi}r^5}. \tag{3}$$

Notably, if the value of the parameter r which is the variance of the Gaussian function variance is fixed, the final response map of an image is obtained by combining the outcomes of individual SFs with different values of θ. In this study, the values of θ vary from $0°$ to $360°$ with an interval of $30°$. The responses of SFs of images containing defects are demonstrated in Figure 1 with different values of the Gaussian function variance.

In addition, the final response map created by SFs for an image I is calculated using the equation below:

$$R(x, y) = F(x, y, \sigma, \theta) * I(x, y), \tag{4}$$

where "$*$" is the symbol of the convolution operator.

2.1.2. Projection Integral (PI). PI is a widely used method for image analysis. This approach is particularly useful for shape and texture categorization and has been extensively employed for face and facial recognition [39, 40]. In the field of civil engineering, this image analysis method has been successfully applied in pavement crack classification tasks [27, 38, 41] as well as pavement pothole recognition [28].

The two PIs along the horizontal and vertical axes of an image are denoted as horizontal PI (HPI) and vertical PI (VPI). These two PIs are computed according to the following equations:

$$HPI(y) = \sum_{i \in x_y} I(i, y),$$

$$VPI(x) = \sum_{j \in y_x} I(x, j), \tag{5}$$

where x_y and y_x are the set of horizontal pixels at the location y and the set of vertical pixels at the location x, respectively (Figure 2).

Since HPI and VPI are incapable of detecting diagonal cracks [42], the two diagonal PIs (DPIs) of an image are employed. The directions of the two DPs, denoted as DPI1 and DPI2, are illustrated in Figure 3. The two DPIs are calculated as follows:

$$DPI1(x, y) = \sum_{x, y \in D1} I(x, y),$$

$$DPI2(x, y) = \sum_{x, y \in D2} I(x, y), \tag{6}$$

where $D1$ and $D2$ are the set of pixels along the two diagonal directions of an image (as illustrated in Figure 3).

As illustrated in Figure 4, images containing diagonal cracks have PIs in which there are exceptionally high intensities in the two DPIs. In addition, as can be shown in Figure 5, HPI and VPI have the strongest responses of PI in images having longitudinal and transverse cracks. On the other hand, an image containing a spall damage results in PIs which do not have a significant peak of signal and the average value of its SF response is higher than that of an image without defective areas.

2.2. Support Vector Machine and Least Squares Support Vector Machine.

Support vector machine (SVM) is a machine learning based classifier which is established on the basis of the statistical learning theory [43]. The aim of this learning algorithm is to find a predictive function based on the collected data set. The standard version of SVM is designed to cope with binary or two-class pattern-recognition problems. Through the model construction phase, SVM constructs a hyperplane to classify data points so that the distance from it to the nearest data sample of each class label is maximized [44].

Moreover, this algorithm relies on the kernel trick to better deal with nonlinearly separable cases. Using the kernel trick, the data points are mapped from an original input space to a high-dimensional feature space so that linear separability is easier to achieve (Figure 6). Superior
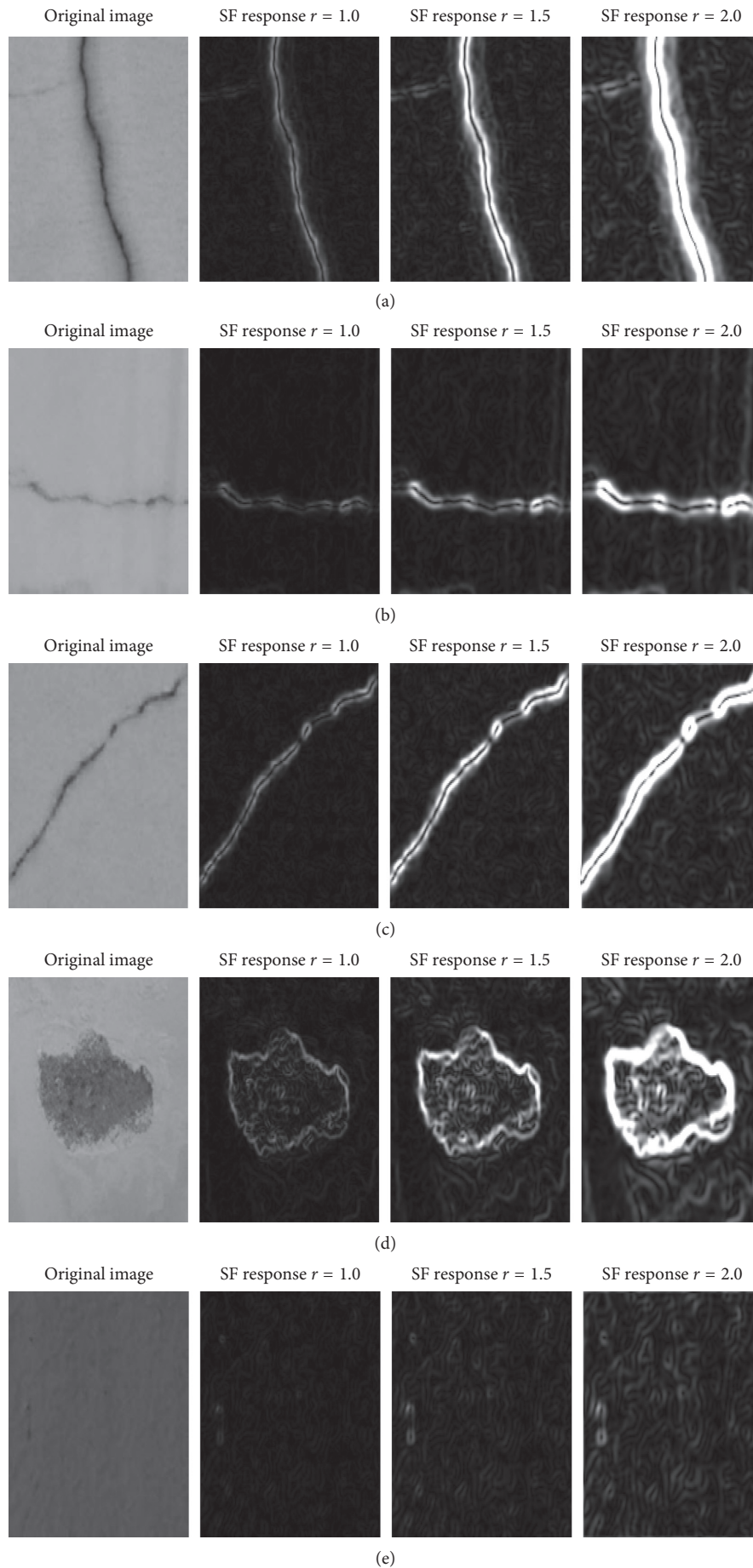
FIGURE 1: SF responses: (a) longitudinal crack, (b) transverse crack, (c) diagonal crack, (d) spall damage, and (e) intact wall.
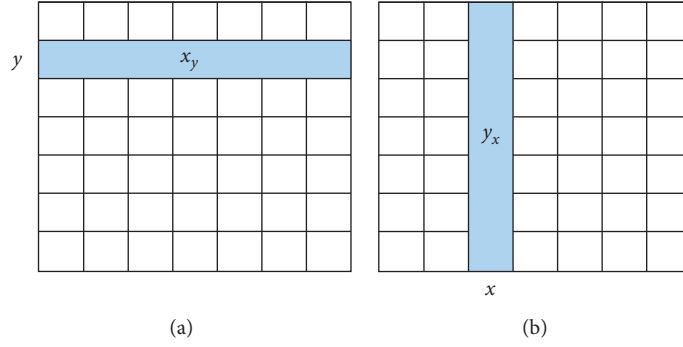
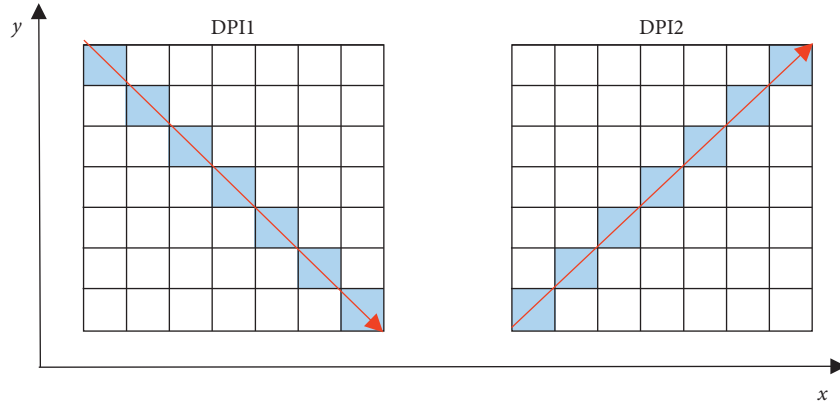FIGURE 2: Illustration of PIs of an image: (a) HPI and (b) VPI.

FIGURE 3: Illustration of DPIs of an image.

classification performance of SVM has been widely reported in a large number of previous studies [45–49].

Given a set of training data points $\{x_k, y_k\}_{k=1}^{N}$ with input data $x_k \in R^n$ and a set of class labels $y_k \in \{-1, +1\}$, the model construction phase of SVM is equivalent to solving the following optimization problem:

$$\text{minimize} \quad J_p(w, e) = \frac{1}{2}w^T w + c\frac{1}{2}\sum_{k=1}^{N} e_k^2,$$

$$\text{subject to} \quad y_k\left(w^T \varphi(x_k) + b\right) \geq 1 - e_k, \quad k = 1, \ldots, N, e_k \geq 0, \tag{7}$$

where $w \in R^n$ and $b \in R$ denote the model parameters, $e_k > 0$ represents a slack variable, c denotes a penalty constant which determines severity of learning error, and $\varphi(x)$ denotes a nonlinear mapping from the input space to the feature space.

One of the advantages of SVM is that it does not require expressing the mapping function $\varphi(x)$ explicitly. Due to the concept of kernel trick, the model identification only necessitates the computation of the kernel function $K(.)$ which is the dot product of $\varphi(x)$. The kernel function is shown below:

$$K(x_k, x_l) = \varphi(x_k)^T \varphi(x_l). \tag{8}$$

Radial basis function (RBF) is often selected to be used in SVM [30]; its formula is given as follows:

$$K(x_k, x_l) = \exp\left(-\frac{\|x_k - x_l\|^2}{2\sigma^2}\right), \tag{9}$$

where σ denotes the kernel function parameter.

To solve the aforementioned constrained optimization, the Lagrangian is given as follows:

$$L(w, b, e; \alpha; v) = J_p(w, e) - \sum_{k=1}^{N} \alpha_k\left\{y_k\left(w^T \varphi(x_k) + b\right) - 1 + e_k\right\}$$

$$- \sum_{k=1}^{N} v_k e_k, \tag{10}$$

where $\alpha_k \geq 0$, $v_k \geq 0$ denote Lagrange multipliers for $k = 1, 2, \ldots, N$.

Accordingly, the conditions for optimality are stated as follows:

$$\begin{cases} \dfrac{\partial L}{\partial w} = 0 \longrightarrow w = \sum_{k=1}^{N} \alpha_k y_k \varphi(x_k), \\[4mm] \dfrac{\partial L}{\partial b} = 0 \longrightarrow \sum_{k=1}^{N} \alpha_k y_k = 0, \\[4mm] \dfrac{\partial L}{\partial e_k} = 0 \longrightarrow 0 \leq \alpha_k \leq c, \quad k = 1, \ldots, N. \end{cases} \tag{11}$$
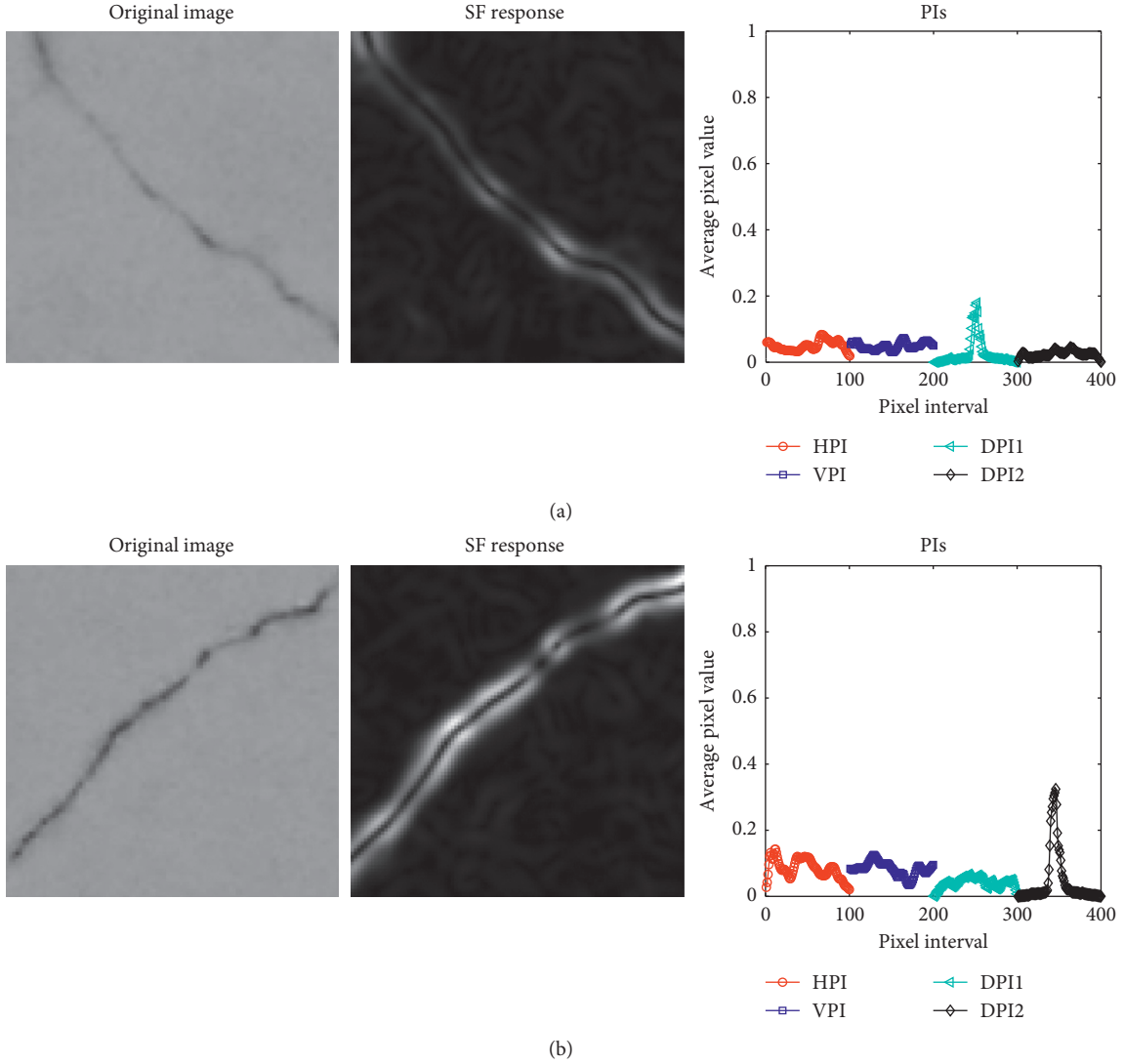
(a)

(b)

Figure 4: PIs of diagonal cracks.

Based on the equations found by the conditions for optimality, it is able to attain the following dual quadratic programming problem:

$$\max_{\alpha} \quad J_D(\alpha) = -\frac{1}{2} \sum_{k,l=1}^{N} y_k y_l \varphi(x_k)^T \varphi(x_l) \alpha_k \alpha_l + \sum_{k=1}^{N} \alpha_k, \tag{12}$$

Subject to $\quad \sum_{k=1}^{N} \alpha_k y_k = 0, \quad 0 \le \alpha_k \le c, \ k = 1, \ldots, N,$

In addition, the kernel function is applied in the following manner:

$$\omega = y_k y_l \varphi(x_k)^T \varphi(x_l) = y_k y_l K(x_k, x_l). \tag{13}$$

Finally, the classification model based on SVM can be derived as follows:

$$y(x) = \text{sign}\left(\sum_{k=1}^{SV} \alpha_k y_k K(x_k, x_l) + b \right), \tag{14}$$

where SV is the number of support vectors which are training data points that have $\alpha_k > 0$.

Least squares support vector machine (LSSVM) [50] is a least square version of the original SVM. Instead of solving a quadratic programming problem required by SVM, the model construction phase of LSSVM is equivalent to solving a system of linear equation. Therefore, the computational expense of LSSVM can be much lower than that of the standard SVM.

To construct a LSSVM based classifier, it is needed to solve the following minimization problem:

$$\text{minimize} \quad J_p(w, e) = \frac{1}{2} w^T w + \gamma \frac{1}{2} \sum_{k=1}^{N} e_k^2,$$

$$\text{subject to} \quad y_k \left(w^T \varphi(x_k) + b \right) = 1 - e_k, \quad k = 1, \ldots, N, \tag{15}$$

where $w \in R^n$ and $b \in R$ are also the model parameters; $e_k \in R$ denote error variables; $\gamma > 0$ is called a regularization constant.
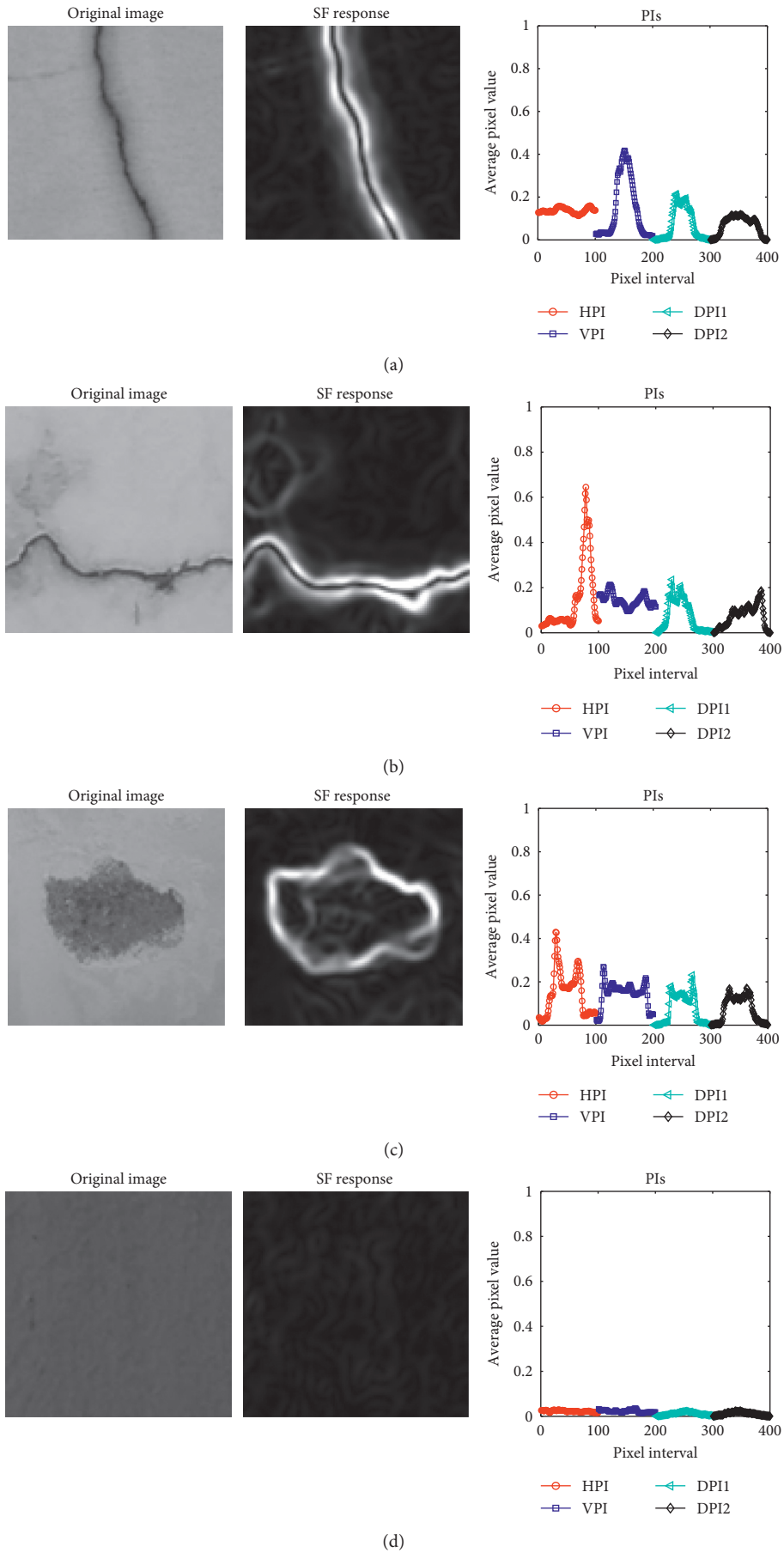
Figure 5: PIs of image samples: (a) longitudinal crack, (b) transverse crack, (c) spall damage, and (d) intact wall.
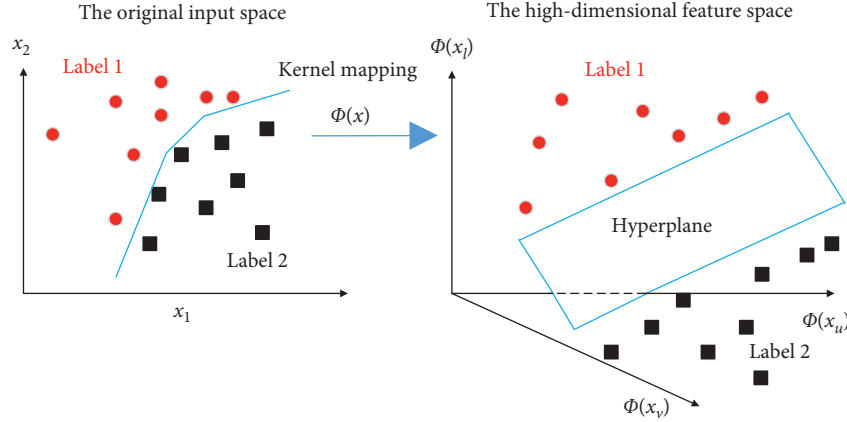
FIGURE 6: The learning phase of SVM.

Subsequently, the Lagrangian is applied in the following way:

$$L(w,b,e;\alpha) = J_p(w,e) - \sum_{k=1}^{N} \alpha_k \left\{ y_k \left(w^T \varphi(x_k) + b \right) - 1 + e_k \right\},$$

(16)

where α_k is the kth Lagrange multiplier; $\varphi(x_k)$ represents a nonlinear mapping function.

Relied on the KKT conditions for optimality, it is able to convert the aforementioned constrained optimization problem to a linear system [51]. The classifier based on LSSVM is compactly expressed as follows:

$$y(x) = \text{sign}\left(\sum_{k=1}^{N} \alpha_k y_i K(x_k, x_l) + b \right),$$

(17)

where α_k and b are found by solving a linear system. Similar to the standard SVM, $K(x_k, x_l)$ denotes the kernel function.

3. Image Sample Collection

Because the machine learning algorithms of SVM and LSSVM are supervised learning approach, a set of wall images with the corresponding ground truth labels must be prepared in advance of the model construction and classification phases. To establish the required data set, images of walls have been collected during field surveys at high-rise buildings in Da Nang city (Vietnam).

To ease the computational process, the size of each image sample is fixed to be 200 × 200 pixels. Moreover, there are five classes of wall condition, namely, longitudinal cracks (LC), transverse crack (TC), diagonal cracks (DC), spall damage (SD), and intact wall (IW). The number of image samples in each class is 100. Thus, the collected image data set contains 500 samples and is illustrated in Figure 7. It is also noted that all the image samples have been preprocessed by the median filter with a window size of 5 × 5 pixels. This preprocessing step aims at suppressing the noise existing in the collected digital image [52]. In addition, the data set is divided into two folders that contain the training set of images (90%) and the testing set of images (10%). The first set

is used in the phase of model construction and the second set is utilized to verify the generalization capability of the wall defect classification model.

4. The Proposed Hybrid Approach of Image Processing and Machine Learning for Detection of Wall Defects

This section describes the proposed model used for automatic classification of wall defects. The overall model structure is illustrated in Figure 8. The model can be divided into two separated modules:

(i) Feature extraction phase that employs the image processing methods of SFs and IPs

(ii) Machine learning based classification phase that relies on the SVM and LSSVM algorithms

In the first step of feature extraction, SFs are employed to compute a salient defect map from a digital image. The minimum and maximum angles of SFs are 0° and 360°, respectively. The parameter r of SFs is selected from a set of [1.0, 1.5, 2.0, 2.5, 3.0]. The value of r which results in the highest accuracy for the training data set is selected as the optimal one. Based on the map generated by SFs, PIs including HPI, VPI, DPI1, and DPI2 are then computed to characterize the texture of the captured images. As earlier mentioned, each image of the data set has the size of 200 × 200 pixels. Thus, each PI contains 200 sampled points and the total number of features to be analyzed by the machine learning algorithm is 200 × 4 = 800. Herein, 4 is the number of PIs.

Obviously, the original PIs can be very rough and have many peaks and valleys due to local fluctuations of the gray intensity of an image. Moreover, the large number of input features can create difficulty for the machine learning algorithms of SVM and LSSVM due to the curse of dimensionality [53]. Therefore, it is beneficial to smooth the original PIs by the use of moving average method [42]. In detail, the average value of W_{PI} consecutive values along the PIs is calculated to create smoothed PIs with fewer data points. For example, if $W_{PI} = 10$, then the total number of
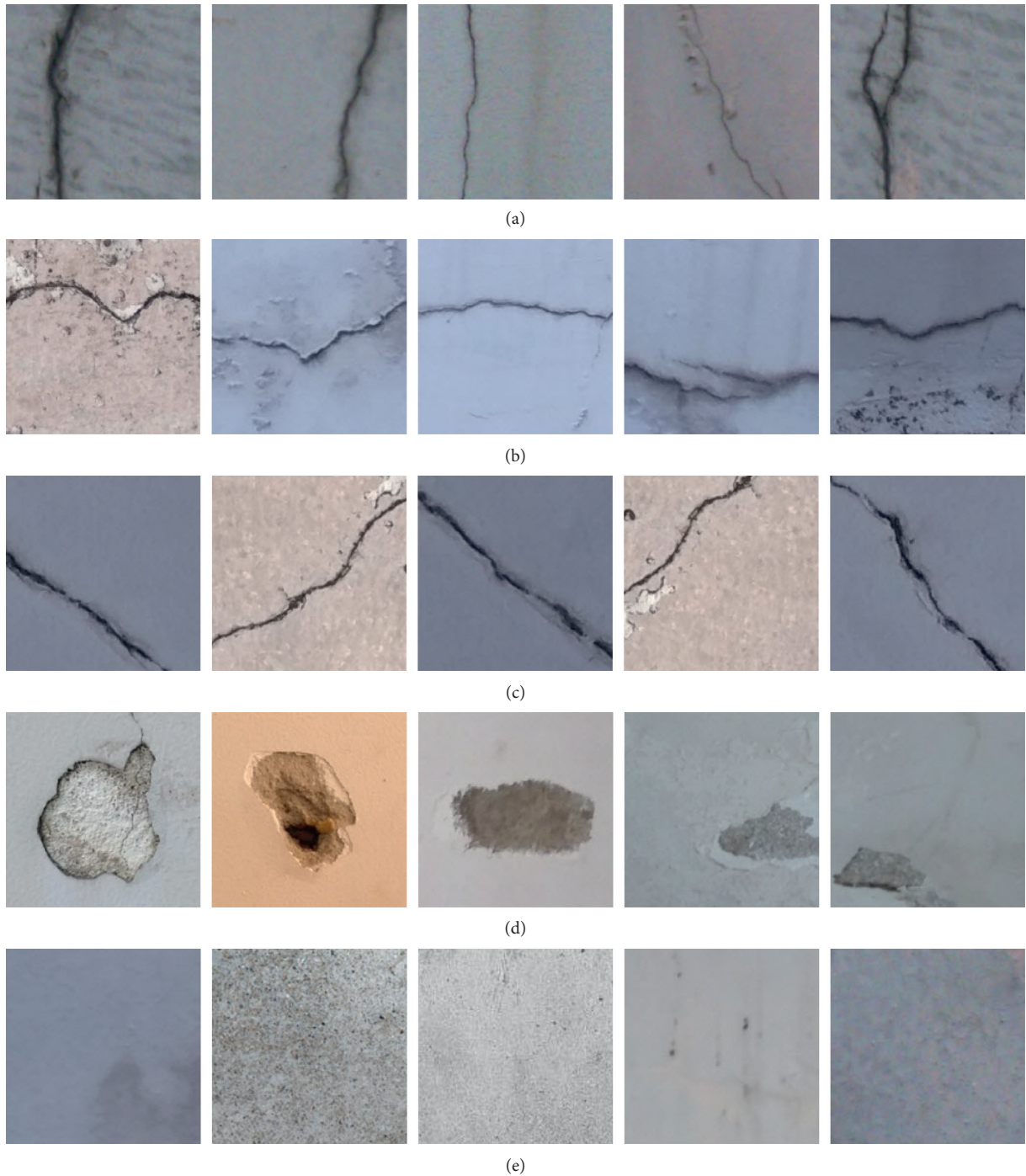
(a)

(b)

(c)

(d)

(e)

FIGURE 7: The collected image samples: (a) longitudinal crack, (b) transverse crack, (c) diagonal crack, (d) spall damage, and (e) intact wall.

features in the contracted PIs is reduced from 800 to 80; if $W_{PI} = 20$, then the machine learning algorithms only have to deal with a data set having 40 features.

The process of feature number reduction using moving average for an image is demonstrated in Figure 9. As can be seen from this example, the smoothed PIs even with the window size $W_{IP} = 20$ still preserve crucial features of rises and ebbs of the original PIs. Therefore, the value of $W_{IP} = 20$ is selected for the feature extraction step. Accordingly, the set of 40 features extracted from PIs is used as input pattern

to categorize the four labels of wall defect (LC, TC, DC, and SD) and the label of intact wall (IW).

Furthermore, to obtain the two DPIs of DPI1 and DPI2, the original map of the SF response has been rotated with the angles of +45 and −45 [42]. Accordingly, the two DPIs are derived from the computation of the HPIs of the two rotated SF maps. The process of computing DPIs of images containing diagonal cracks is demonstrated in Figure 10. In addition, the overall feature extraction module is depicted in Figure 11. Based on the 40 input features (IF) extracted from
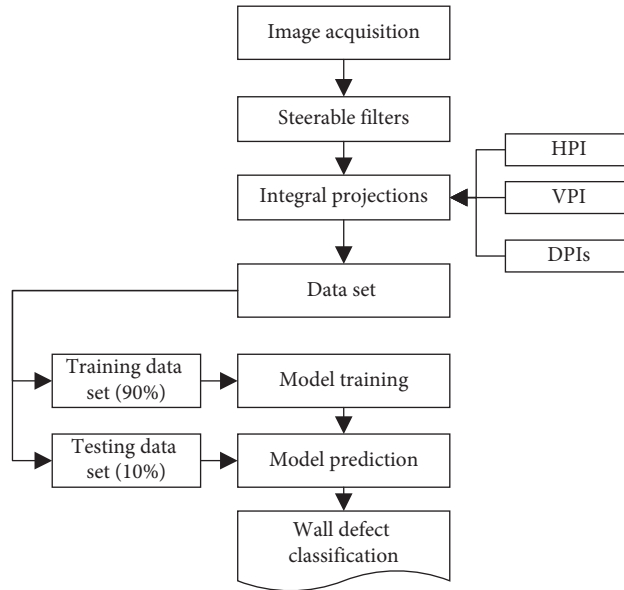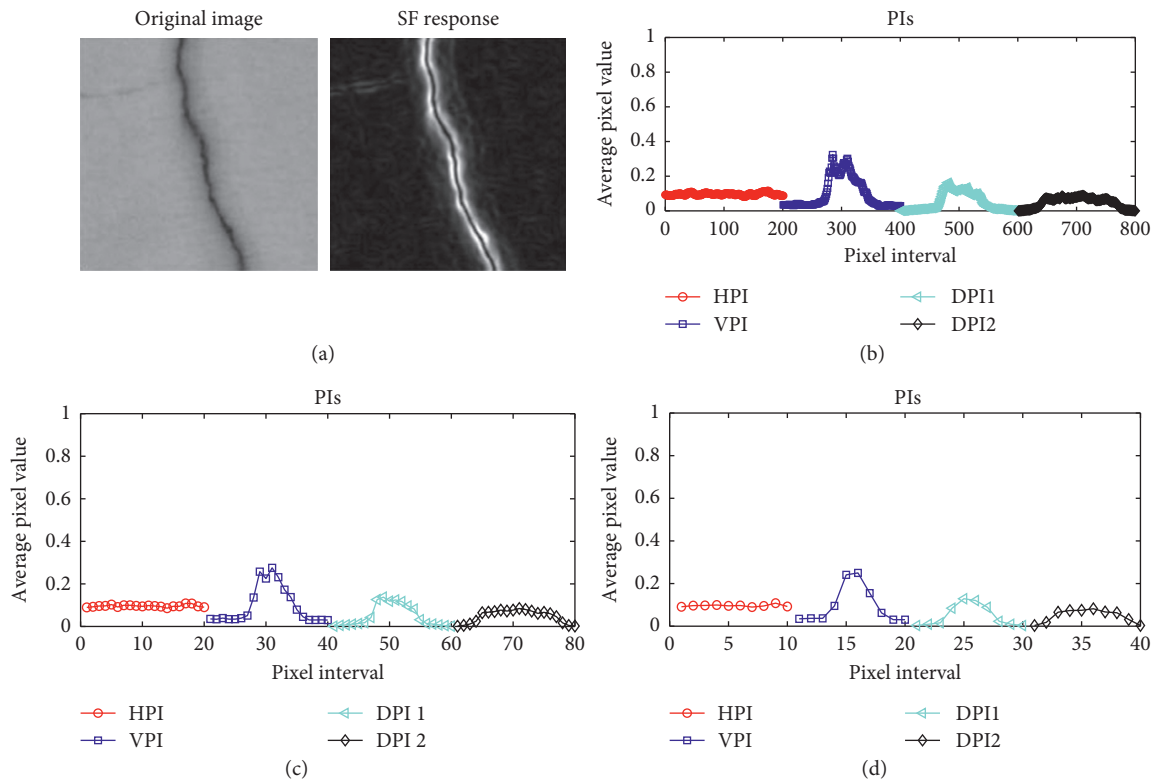
FIGURE 8: The proposed model structure.

FIGURE 9: PIs of an image: (a) the original image, (b) the original PIs ($W_{PI} = 1$), (c) the smoothed PIs ($W_{PI} = 10$), and (d) the smoothed PIs ($W_{PI} = 20$).

the PIs, the machine learning algorithms of SVM and LSSVM are employed to perform the model learning and classification of images in the second module of the model.

It is noted that the standard versions of SVM and LSSVM are designed two-class pattern recognition problems. Hence, the one-versus-one (OvO) strategy [54] has been used with SVM and LSSVM to make them capable of dealing with the five-class recognition tasks at hand. Previous works have confirmed the advantages of OvO strategy in coping with multiclass classification problems [53, 55, 56].
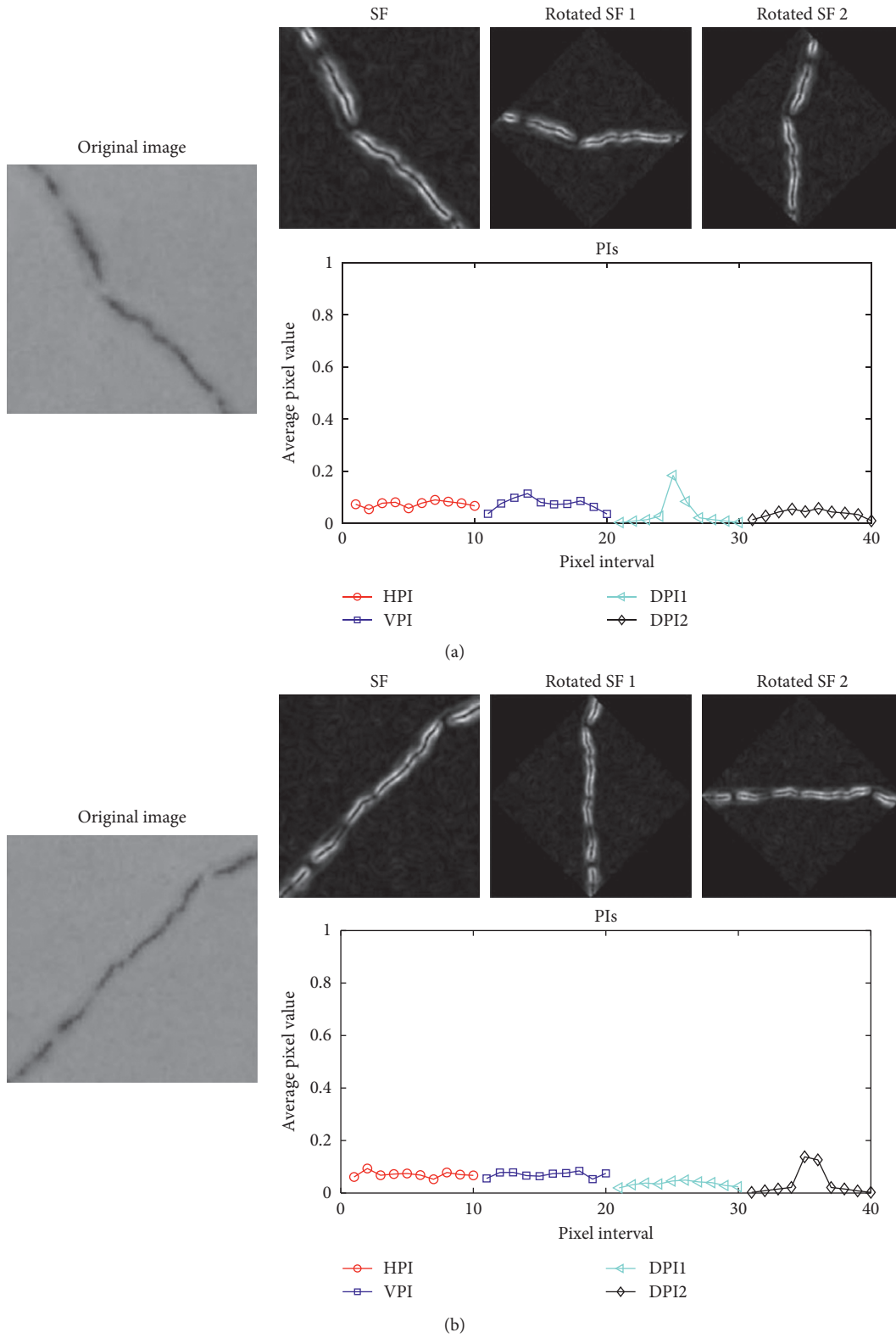
FIGURE 10: The process of computing DPIs: (a) a −45° diagonal crack and (b) a + 45° diagonal crack.

Input image

SF

Rotated SFs

The smoothed PIs

PIs

The original PIs

PIs

- HPI
- VPI
- DPI1
- DPI2

- HPI
- VPI
- DPI1
- DPI2

The extracted feature used for pattern classification

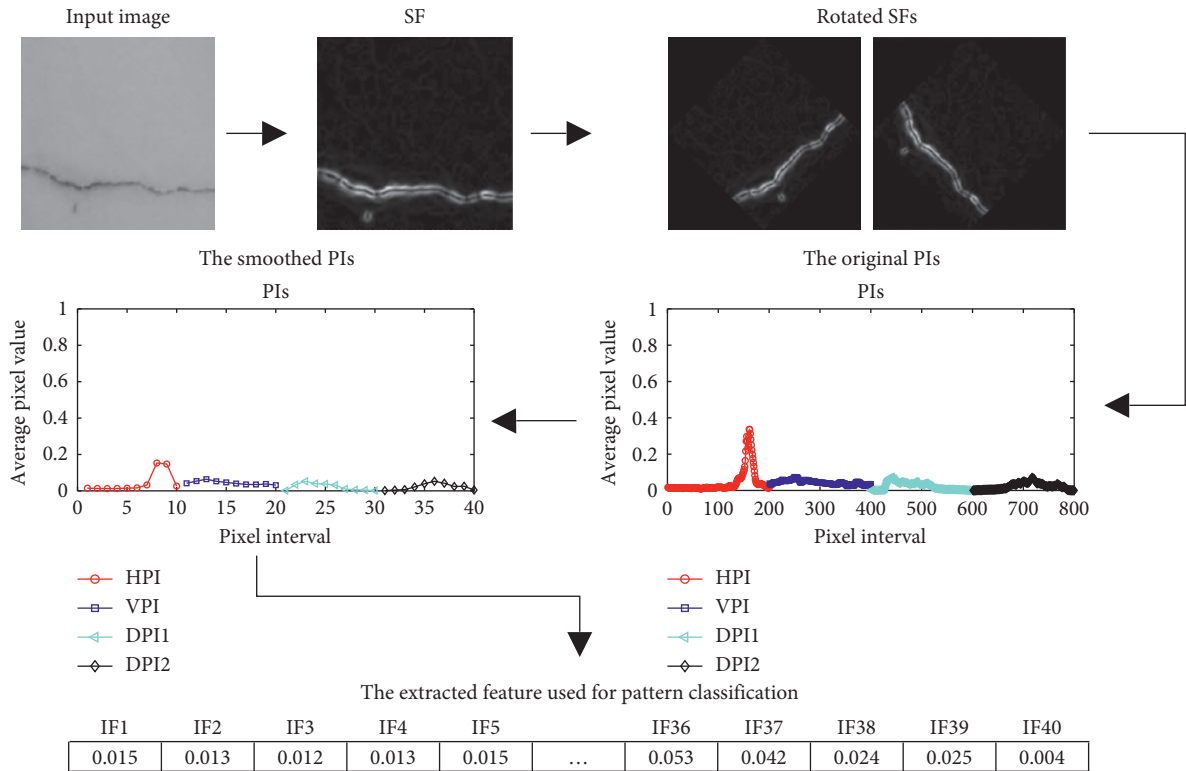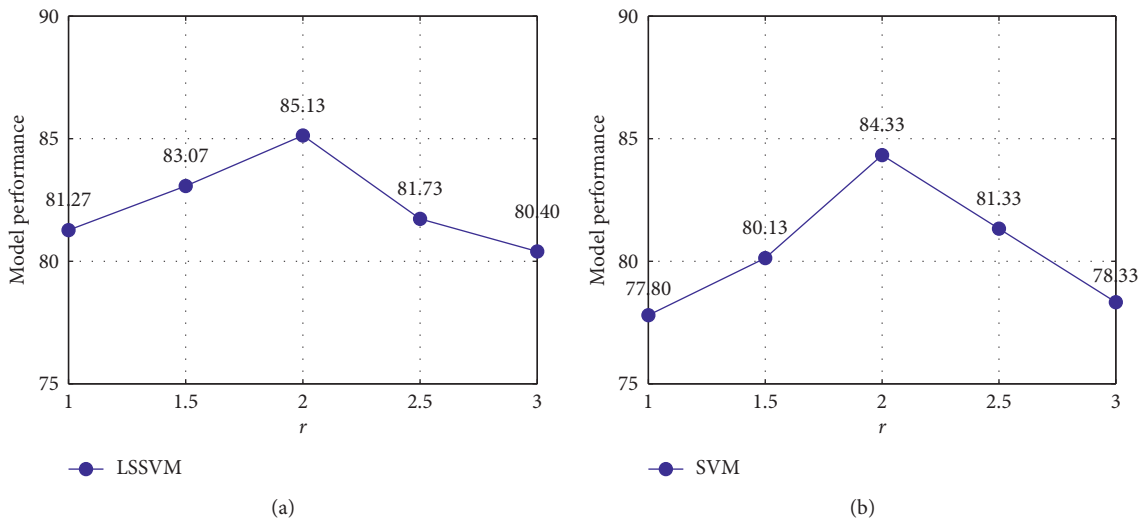| IF1	IF2	IF3	IF4	IF5		IF36	IF37	IF38	IF39	IF40
0.015	0.013	0.012	0.013	0.015	...	0.053	0.042	0.024	0.025	0.004

FIGURE 11: The whole feature extraction process.

(a)

(b)

FIGURE 12: Model performance with different values of the parameter r: (a) LSSVM and (b) SVM.

5. Experimental Results

Because the detection of wall defects is formulated as a five-class pattern recognition problem, classification accuracy rate (CAR) computed for each individual class and for all of the classes is employed. CAR for the class i is computed as follows:

$$\text{CAR}_i = \frac{R_C^i}{R_A^i} \times 100\,(\%), \tag{18}$$

where R_C^i and R_A^i denote the number of data samples in class ith being correctly classified and the total number of data instances in this class, respectively. It is reminded that that there are five class labels in the data set: longitudinal crack (LC), transverse crack (TC), diagonal crack (DC), spall damage (SD), and intact wall (IW).

The overall classification accuracy rate (CAR) for all the five class labels is simply computed as follows:

TABLE 1: Result comparison.

| Statistics	CAR (%)	Classification models					
		LSSVM	SVM	BPANN	CT	LDA	NBC
Average	CAR_{LC}	85.33	79.00	79.33	67.00	74.33	73.00
	CAR_{TC}	83.00	75.67	77.33	68.67	74.67	72.67
	CAR_{DC}	90.00	94.67	63.67	62.67	53.00	54.67
	CAR_{SD}	78.33	84.33	69.33	55.33	31.33	26.00
	CAR_{IW}	89.00	88.00	81.33	57.67	74.67	72.33
	CAR_{O}	85.13	84.33	74.20	62.27	61.60	59.73
Std.	CAR_{LC}	10.42	12.69	11.12	16.01	17.94	13.43
	CAR_{TC}	10.22	15.24	17.21	13.83	12.24	11.43
	CAR_{DC}	11.74	7.30	14.26	13.11	16.43	17.56
	CAR_{SD}	13.41	11.35	17.80	16.97	15.02	12.76
	CAR_{IW}	10.62	8.05	13.58	18.88	12.79	13.05
	CAR_{O}	5.89	5.28	6.75	5.80	6.53	5.63
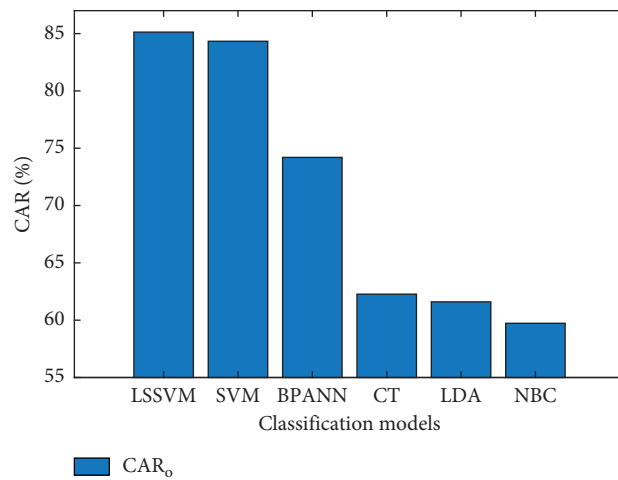
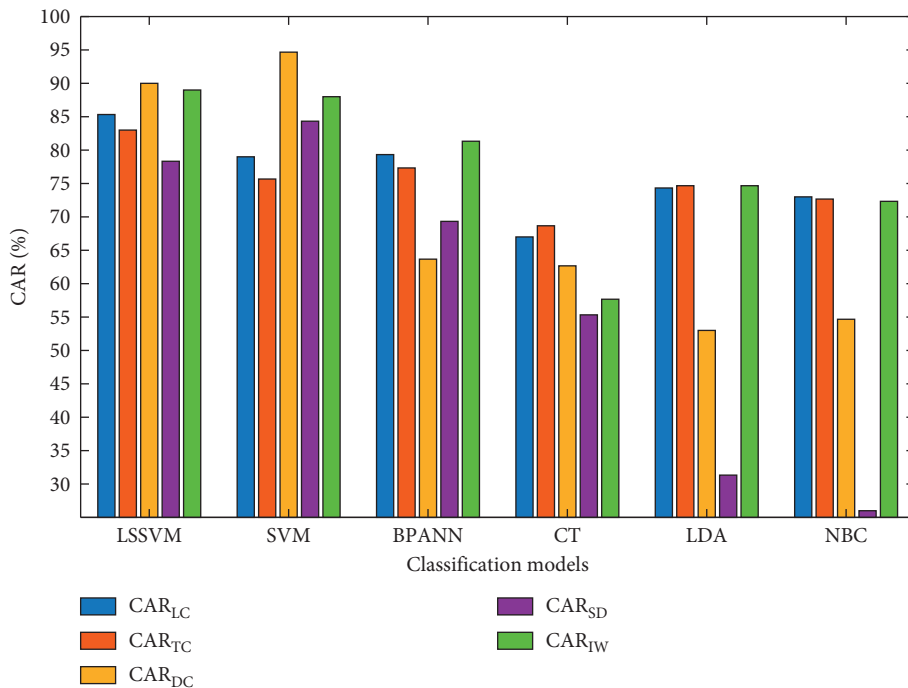FIGURE 13: Result comparison based on CAR_O.

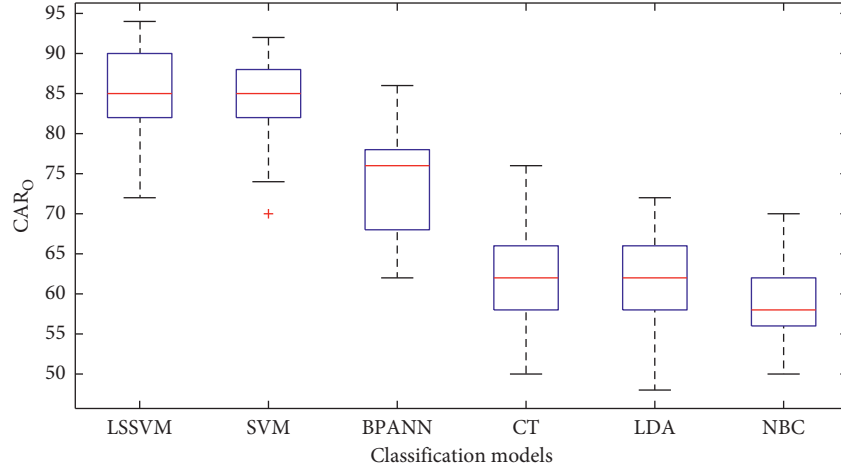FIGURE 14: Classification accuracy comparison based on CAR of each class (LD, TC, DC, SD, and IW).

FIGURE 15: Box plots of overall CARs.

TABLE 2: p values of the Wilcoxon signed-rank test.

	LSSVM	SVM	BPANN	CT	LDA	NBC
LSSVM	0.00000	0.60134	0.00001	0.00000	0.00000	0.00000
SVM	0.60134	0.00000	0.00002	0.00000	0.00000	0.00000
BPANN	0.00001	0.00002	0.00000	0.00000	0.00000	0.00000
CT	0.00000	0.00000	0.00000	0.00000	0.06728	0.00444
LDA	0.00000	0.00000	0.00000	0.06728	0.00000	0.02230
NBC	0.00000	0.00000	0.00000	0.00444	0.02230	0.00000

$$\text{CAR}_{\text{Overall}} = \sum_{i=1}^{5} \frac{\text{CAR}_i}{5}. \qquad (19)$$

As stated earlier, the data set including 500 samples is employed to train and test the wall defect classification model. This data set is randomly separated into two subsets: data for model training (90%) and data for testing (10%). Because a single run of model training and testing may not help to reveal the true performance of a classifier, this study performs a repeated subsampling process that includes 20 times of model training and prediction. In each time of running, 10% of the data set is randomly extracted to form the testing data subset; the rest of the data set is reserved for model testing phase.

As described in the formulation of the two machine learning algorithms of SVM and LSSVM, these two algorithms both require a proper setting of their tuning parameters. In the case of SVM, the tuning parameters are the penalty coefficient and the kernel function parameter. In the case of LSSVM, the regularization and the kernel function parameters need to be selected appropriately. In this section, the grid search method described in the previous work of [57] is employed for automatically setting those tuning parameters of SVM and LSSVM. In addition, the feature selection stage requires the setting of the parameter r in the computation of SFs. The model performance with different values of the parameter r for the cases of SVM and LSSVM is reported in Figure 12. As can be observed from this figure,

$r = 2$ results in the highest $\text{CAR}_{\text{Overall}}$ values for both SVM and LSSVM.

Besides the two machine learning algorithms of SVM and LSSVM, the backpropagation artificial neural network (BPANN), classification tree (CT), linear discriminant analysis (LDA), and naive Bayes classifier (NBC) are also employed as benchmark classifiers. It is also noted that CT, LDA, and NBC are also equipped with the OvO strategy to deal with the current five-class recognition problem of wall defect classification. The SVM and the benchmark algorithms implemented in MATLAB with the help of the statistics and machine learning toolbox [58]. In addition, the LSSVM model is constructed by the built-in functions provided in the toolbox developed by De Brabanter et al. [59].

In addition, the training phases of BPANN and CT require a proper setting of their model hyper-parameters. Similar to the cases of SVM and LSSVM, the model hyper-parameters of those models that result in the best performance for the testing set are selected. In the case of the DT model, the suitable value of the minimal number of observations per tree leaf is found to be 2. The appropriate structure of the BPANN model consists of 35 neurons in the hidden layers; furthermore, the scaled conjugate gradient algorithm with the maximum number of training epochs = 3000 is used to train the neural network model. Moreover, the processes of selecting an appropriate value of the tuning parameter r used in constructing the SF maps of the benchmark models of BPANN, CT, LDA, and NBC are
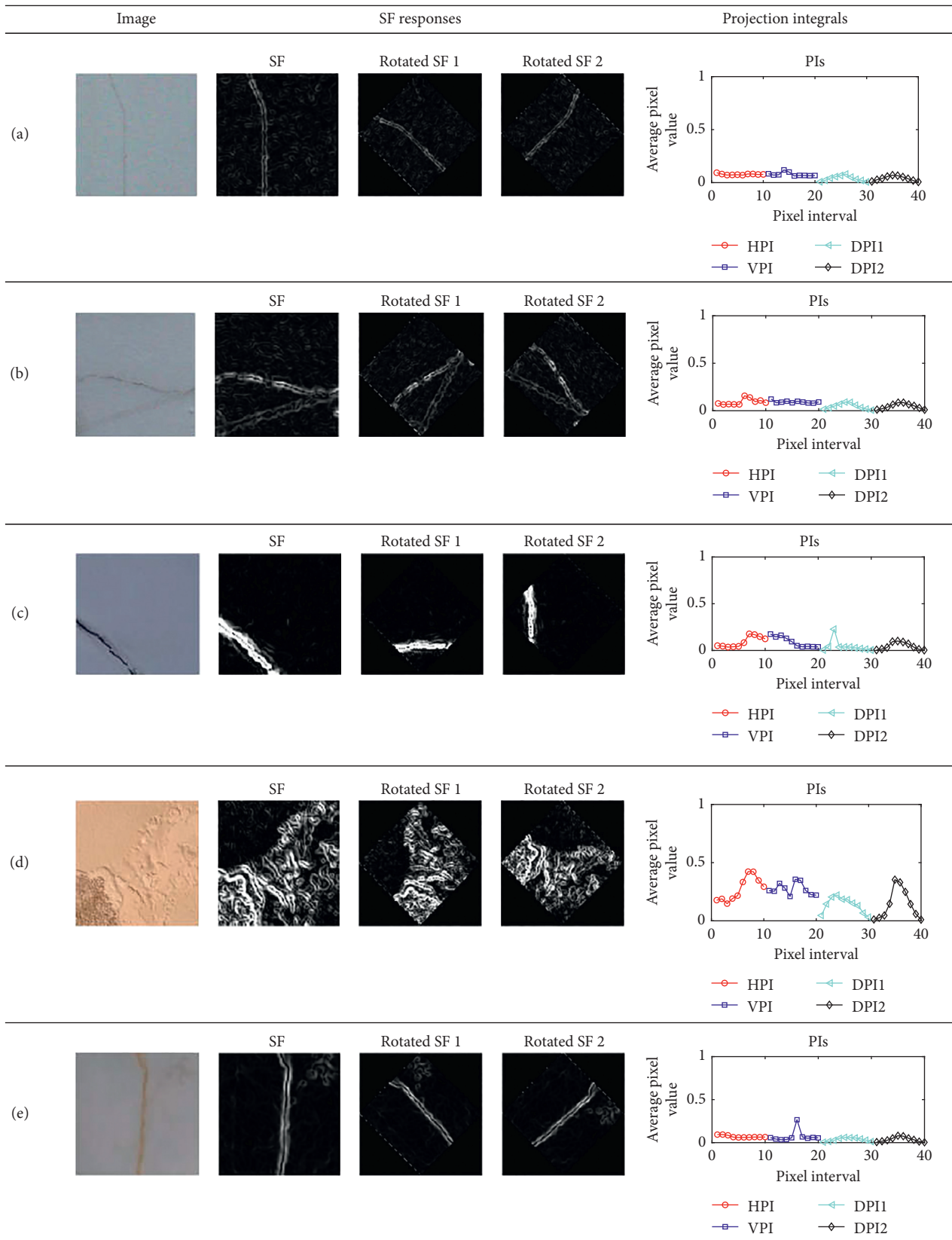
FIGURE 16: Examples of incorrect classifications.

similar to those of the SVM and LSSVM models. Based on result comparisons, the suitable value of the tuning parameter r used with BPANN, CT, LDA, and NBC is also 2.

The performances of the machine learning classifiers used for wall damage recognition are summarized in Table 1. Observed from this table, LSSVM has achieved the best predictive performance in terms of CAR_o (85.13%), followed by SVM ($CAR_o = 84.33\%$), BPANN ($CAR_o = 74.20\%$), CT ($CAR_o = 62.27\%$), LDA ($CAR_o = 61.00\%$), and NBC ($CAR_o = 59.73\%$). Thus, it can be seen that classifiers based on LSSVM and SVM are more suitable for the task of wall defect classification than other machine learning and statistical approaches of BPANN, CT, LDA, and NBC.

Figures 13 and 14 graphically compare the results obtained from the prediction models in terms of CAR_o and CAR of each individual class label. It is shown that the CARs of LC (85.33%), TC (83.00%), and IW (89.00%) obtained from LSSVM are higher than those yielded by SVM (79.00%, 75.67%, and 88.00% for the LC, TC, and IW, respectively). However, results of SVM for the classes of DC (94.67%) and SD (84.33%) are better than those of LSSVM (90.00% and 78.33% for the classes of DC and SD, respectively).

In addition, the classification results of all the models in terms of CAR_o are displayed by the box plots in Figure 15. Moreover, to better demonstrate the statistical difference between each pair of classifiers employed in the task of wall defect recognition, the Wilcoxon signed-rank test (WSRT) is utilized in this section. WSRT is a nonparametric statistical hypothesis test that is widely used for verifying the statistical difference of model performances [57]. With the significance level of the test = 0.05, if p value computed from the test is smaller than 0.05, it can be confirmed that the performances of the two selected classifiers are statistically different. The p values obtained from WSRT for each pair of classifiers are reported in Table 2. The outcomes shown in this table confirm that LSSVM and SVM are significantly better than other benchmark models in the task of recognizing wall damages. In addition, with p values = 0.60134, there is no statistical difference between the performances of LSSVM and SVM.

Although the LSSVM model has delivered the highest CARs, this model also commits wrong classification cases. These misclassifications are investigated and examples of them are illustrated in Figure 16. In Figures 16(a) and 16(b), images with the ground truth label of LC and TC have been assigned the label of IW. The reasons for these misclassifications are that the crack objects are too thin; moreover, there is a line of stain existing in Figure 16(b). The case in Figure 16(c) shows an image with its ground truth class of DC which has been categorized as the class of TC. The possible reason of this phenomenon is that the crack object appears too close to corner of the image; therefore, the signals of the SF responses of the two DPIs are not significantly stronger than those of other PIs. In Figure 16(d), an image with complex background texture has caused the machine to misclassify an image with the ground truth category of SD. Moreover, an object of stain (Figure 16(e)) leads to the classification of an image into the class of LC while it actually belongs to the class of IW.

6. Conclusion

This study has proposed an automatic approach for periodic survey of concrete wall structures. The newly constructed approach mainly consists of the feature extraction step and the pattern classification step. In the first step, image processing techniques of SF and PI have been employed to characterize the texture and the pattern existing in images. In the second step, machine learning algorithms of SVM and LSSVM have been used to analyze the features extracted by the image processing techniques and to assign input images into one of the five class labels of LC, TC, DC, SD, and IW. Experimental results using a repeated random subsampling with 20 runs show that the predictive performances of LSSVM ($CAR_o = 85.13\%$) and SVM ($CAR_o = 84.33\%$) are superior to other benchmark models of BPANN, CT, LDA, and NBC. These facts confirm that the proposed approach can be a time- and cost-effective solution for the task of building periodic survey. The future developments of the current study include the integration of other advanced image processing methods (e.g., image segmentation, color/texture analyses) to enhance the CARs via the reduction of falsely classified cases.

Data Availability

The data used to support the findings of this study are available from the corresponding author upon request.

Conflicts of Interest

The author declares that there are no conflicts of interests regarding the publication of this research work.

Supplementary Materials

The supplementary file contains the data set used in this study. In this file, the first 500 columns are the input features (X1 to X40) of the data (which are the smoothed projection integrals); the last column is the class labels (1 = longitudinal crack, 2 = transverse crack, 3 = diagonal crack, 4 = spall damage, and 5 = intact wall). (*Supplementary Materials*)

References

[1] W. Zhang, Z. Zhang, D. Qi, and Y. Liu, "Automatic crack detection and classification method for subway tunnel safety monitoring," *Sensors*, vol. 14, no. 10, pp. 19307–19328, 2014.

[2] Y.-J. Cha, W. Choi, G. Suh, S. Mahmoudkhani, and O. Büyüköztürk, "Autonomous structural visual inspection using region-based deep learning for detecting Multiple damage types," *Computer-Aided Civil and Infrastructure Engineering*, vol. 33, no. 9, pp. 731–747, 2018.

[3] T. Dawood, Z. Zhu, and T. Zayed, "Machine vision-based model for spalling detection and quantification in subway networks," *Automation in Construction*, vol. 81, pp. 149–160, 2017.

[4] S. German, I. Brilakis, and R. DesRoches, "Rapid entropy-based detection and properties measurement of concrete spalling with machine vision for post-earthquake safety

assessments," *Advanced Engineering Informatics*, vol. 26, no. 4, pp. 846–858, 2012.

[5] M.-K. Kim, H. Sohn, and C.-C. Chang, "Localization and quantification of concrete spalling defects using terrestrial laser scanning," *Journal of Computing in Civil Engineering*, vol. 29, no. 6, article 04014086, 2015.

[6] P. Tang, D. Huber, and B. Akinci, "Characterization of laser scanners and algorithms for detecting flatness defects on concrete surfaces," *Journal of Computing in Civil Engineering*, vol. 25, no. 1, pp. 31–42, 2011.

[7] H. Kim, E. Ahn, M. Shin, and S.-H. Sim, "Crack and noncrack classification from concrete surface images using machine learning," *Structural Health Monitoring*, vol. 0, article 1475921718768747, 2018.

[8] R. Davoudi, G. R. Miller, and J. N. Kutz, "Structural load estimation using machine vision and surface crack patterns for shear-critical RC beams and slabs," *Journal of Computing in Civil Engineering*, vol. 32, no. 4, article 04018024, 2018.

[9] J.-Y. Jung, H.-J. Yoon, and H.-W. Cho, "A study on crack depth measurement in steel structures using image-based intensity differences," *Advances in Civil Engineering*, vol. 2018, Article ID 7530943, 10 pages, 2018.

[10] C. Koch, K. Georgieva, V. Kasireddy, B. Akinci, and P. Fieguth, "A review on computer vision based defect detection and condition assessment of concrete and asphalt civil infrastructure," *Advanced Engineering Informatics*, vol. 29, no. 2, pp. 196–210, 2015.

[11] C. Koch, S. G. Paal, A. Rashidi, Z. Zhu, M. König, and I. Brilakis, "Achievements and challenges in machine vision-based inspection of large concrete structures," *Advances in Structural Engineering*, vol. 17, no. 3, pp. 303–318, 2014.

[12] H. Pragalath, S. Seshathiri, H. Rathod, B. Esakki, and R. Gupta, "Deterioration assessment of infrastructure using fuzzy logic and image processing algorithm," *Journal of Performance of Constructed Facilities*, vol. 32, no. 2, article 04018009, 2018.

[13] Y.-S. Yang, C.-l. Wu, T. T. C. Hsu, H.-C. Yang, H.-J. Lu, and C.-C. Chang, "Image analysis method for crack distribution and width estimation for reinforced concrete structures," *Automation in Construction*, vol. 91, pp. 120–132, 2018.

[14] Z. Zhu, S. German, and I. Brilakis, "Detection of large-scale concrete columns for automated bridge inspection," *Automation in Construction*, vol. 19, no. 8, pp. 1047–1055, 2010.

[15] T. C. Hutchinson and Z. Chen, "Improved image analysis for evaluating concrete damage," *Journal of Computing in Civil Engineering*, vol. 20, no. 3, pp. 210–216, 2006.

[16] L.-C. Chen, Y.-C. Shao, H.-H. Jan, C.-W. Huang, and Y.-M. Tien, "Measuring system for cracks in concrete using multitemporal images," *Journal of Surveying Engineering*, vol. 132, no. 2, pp. 77–82, 2006.

[17] Z. Zhu and I. Brilakis, "Detecting air pockets for architectural concrete quality assessment using visual sensing," *Electronic Journal of Information Technology in Construction*, vol. 13, pp. 86–102, 2008.

[18] Z. Chen and T. C. Hutchinson, "Image-based framework for concrete surface crack monitoring and quantification," *Advances in Civil Engineering*, vol. 2010, Article ID 215295, 18 pages, 2010.

[19] B. Y. Lee, Y. Y. Kim, S.-T. Yi, and J.-K. Kim, "Automated image processing technique for detecting and analysing concrete surface cracks," *Structure and Infrastructure Engineering*, vol. 9, no. 6, pp. 567–577, 2013.

[20] J. Valença, L. M. S. Gonçalves, and E. Júlio, "Damage assessment on concrete surfaces using multi-spectral image analysis," *Construction and Building Materials*, vol. 40, pp. 971–981, 2013.

[21] B. Liu and T. Yang, "Image analysis for detection of bugholes on concrete surface," *Construction and Building Materials*, vol. 137, pp. 432–440, 2017.

[22] H. Kim, E. Ahn, S. Cho, M. Shin, and S.-H. Sim, "Comparative analysis of image binarization methods for crack identification in concrete structures," *Cement and Concrete Research*, vol. 99, pp. 53–61, 2017.

[23] N.-D. Hoang, "Detection of surface crack in building structures using image processing technique with an improved Otsu method for image thresholding," *Advances in Civil Engineering*, vol. 2018, Article ID 3924120, 10 pages, 2018.

[24] W. R. L. de Silva and D. S. d. Lucena, "Concrete cracks detection based on deep learning image classification," *Proceedings*, vol. 2, no. 8, p. 489, 2018.

[25] S. Dorafshan, R. J. Thomas, and M. Maguire, "Comparison of deep convolutional neural networks and edge detectors for image-based crack detection in concrete," *Construction and Building Materials*, vol. 186, pp. 1031–1045, 2018.

[26] Y.-J. Cha, W. Choi, and O. Büyüköztürk, "Deep learning-based crack damage detection using convolutional neural networks," *Computer-Aided Civil and Infrastructure Engineering*, vol. 32, no. 5, pp. 361–378, 2017.

[27] A. Cubero-Fernandez, F. J. Rodriguez-Lozano, R. Villatoro, J. Olivares, and J. M. Palomares, "Efficient pavement crack detection and classification," *EURASIP Journal on Image and Video Processing*, vol. 2017, no. 39, 2017.

[28] N.-D. Hoang, "An artificial intelligence method for asphalt pavement pothole detection using least squares support vector machine and neural network with steerable filter-based feature extraction," *Advances in Civil Engineering*, vol. 2018, Article ID 7419058, 12 pages, 2018.

[29] G. M. Hadjidemetriou, P. A. Vela, and S. E. Christodoulou, "Automated pavement patch detection and quantification using support vector machines," *Journal of Computing in Civil Engineering*, vol. 32, no. 1, article 04017073, 2018.

[30] B. T. Pham, A. Jaafari, I. Prakash, and D. T. Bui, "A novel hybrid intelligent model of support vector machines and the MultiBoost ensemble for landslide susceptibility modeling," *Bulletin of Engineering Geology and the Environment*, 2018, In press.

[31] H. Shin and J. Paek, "Automatic task classification via support vector machine and crowdsourcing," *Mobile Information Systems*, vol. 2018, Article ID 6920679, 9 pages, 2018.

[32] M. Wang, Y. Wan, Z. Ye, and X. Lai, "Remote sensing image classification based on the optimal support vector machine and modified binary coded ant colony optimization algorithm," *Information Sciences*, vol. 402, pp. 50–68, 2017.

[33] Y. Zhou, W. Su, L. Ding, H. Luo, and P. E. D. Love, "Predicting safety risks in deep foundation pits in subway infrastructure projects: support vector machine approach," *Journal of Computing in Civil Engineering*, vol. 31, no. 5, article 04017052, 2017.

[34] G. K. Choudhary and S. Dey, "Crack detection in concrete surfaces using image processing, fuzzy logic, and neural networks," in *Proceedings of 2012 IEEE Fifth International Conference on Advanced Computational Intelligence (ICACI)*, pp. 404–411, Nanjing, China, October 2012.

[35] A. Mohan and S. Poobal, "Crack detection using image processing: a critical review and analysis," *Alexandria Engineering Journal*, vol. 57, no. 2, 2017.

[36] W. T. Freeman and E. H. Adelson, "Steerable filters for early vision, image analysis, and wavelet decomposition," in *Proceedings of Third International Conference on Computer Vision*, pp. 406–415, Osaka, Japan, December 1990.

[37] E. P. Simoncelli and H. Farid, "Steerable wedge filters," in *Proceedings of IEEE International Conference on Computer Vision*, pp. 189–194, Cambridge, MA, USA, June 1995.

[38] N.-D. Hoang and Q.-L. Nguyen, "A novel method for asphalt pavement crack classification based on image processing and machine learning," *Engineering with Computers*, 2018, In press

[39] A. Chouchane, M. Belahcene, and S. Bourennane, "3D and 2D face recognition using integral projection curves based depth and intensity images," *International Journal of Intelligent Systems Technologies and Applications*, vol. 14, no. 1, pp. 50–69, 2015.

[40] A. Hernandez-Matamoros, A. Bonarini, E. Escamilla-Hernandez, M. Nakano-Miyatake, and H. Perez-Meana, "Facial expression recognition with automatic segmentation of face regions using a fuzzy based classification approach," *Knowledge-Based Systems*, vol. 110, pp. 1–14, 2016.

[41] S. Li, Y. Cao, and H. Cai, "Automatic pavement-crack detection and segmentation based on steerable matched filtering and an active contour model," *Journal of Computing in Civil Engineering*, vol. 31, no. 5, article 04017045, 2017.

[42] N.-D. Hoang and Q.-L. Nguyen, "Automatic recognition of asphalt pavement cracks based on image processing and machine learning approaches: a comparative study on classifier performance," *Mathematical Problems in Engineering*, vol. 2018, Article ID 6290498, 16 pages, 2018.

[43] V. N. Vapnik, *Statistical Learning Theory*, John Wiley & Sons, Inc, Hoboken, NJ, USA, 1998, ISBN-10: 0471030031.

[44] L. H. Hamel, *Knowledge Discovery with Support Vector Machines*, John Wiley & Sons, Inc., Hoboken, NJ, USA, 2009, ISBN: 978-0-470-37192-3.

[45] W. L. Al-Yaseen, Z. A. Othman, and M. Z. A. Nazri, "Multi-level hybrid support vector machine and extreme learning machine based on modified K-means for intrusion detection system," *Expert Systems with Applications*, vol. 67, pp. 296–303, 2017.

[46] W. Chen, H. R. Pourghasemi, and S. A. Naghibi, "A comparative study of landslide susceptibility maps produced using support vector machine with different kernel functions and entropy data mining models in China," *Bulletin of Engineering Geology and the Environment*, vol. 77, no. 2, pp. 647–664, 2018.

[47] H. Hasni, A. H. Alavi, P. Jiao, and N. Lajnef, "Detection of fatigue cracking in steel bridge girders: a support vector machine approach," *Archives of Civil and Mechanical Engineering*, vol. 17, no. 3, pp. 609–622, 2017.

[48] B. Kalantar, B. Pradhan, S. A. Naghibi, A. Motevalli, and S. Mansor, "Assessment of the effects of training data selection on the landslide susceptibility mapping: a comparison between support vector machine (SVM), logistic regression (LR) and artificial neural networks (ANN)," *Geomatics, Natural Hazards and Risk*, vol. 9, no. 1, pp. 49–69, 2018.

[49] A. Saxena and S. Shekhawat, "Ambient air quality classification by grey wolf optimizer based support vector machine," *Journal of Environmental and Public Health*, vol. 2017, Article ID 3131083, 12 pages, 2017.

[50] J. A. K. Suykens and J. Vandewalle, "Least squares support vector machine classifiers," *Neural Processing Letters*, vol. 9, no. 3, pp. 293–300, 1999.

[51] J. Suykens, J. V. Gestel, J. D. Brabanter, B. D. Moor, and J. Vandewalle, *Least Square Support Vector Machines*, World Scientific Publishing Co. Pte. Ltd., Singapore, 2002, ISBN-13: 978-9812381514.

[52] H. Rababaah, "Asphalt pavement crack classification: a comparative study of three ai approaches: multilayer perceptron, genetic algorithms, and self-organizing maps," M.S. Thesis, Indiana University South Bend, South Bend, IN, USA, 2005.

[53] C. M. Bishop, *Pattern Recognition and Machine Learning (Information Science and Statistics*, Springer, Berlin, Germany, ISBN-10: 0387310738, 2011.

[54] A. Rocha and S. K. Goldenstein, "Multiclass from binary: expanding one-versus-all, one-versus-one and ECOC-based approaches," *IEEE Transactions on Neural Networks and Learning Systems*, vol. 25, no. 2, pp. 289–302, 2014.

[55] K.-B. Duan, J. C. Rajapakse, and M. N. Nguyen, *One-Versus-One and One-Versus-All Multiclass SVM-RFE for Gene Selection in Cancer Classification*, pp. 47–56, Springer Berlin Heidelberg, Berlin, Heidelberg, 2007.

[56] C.-W. Hsu and C.-J. Lin, "A comparison of methods for multiclass support vector machines," *IEEE Transactions on Neural Networks*, vol. 13, pp. 415–425, 2002.

[57] N.-D. Hoang and D. T. Bui, "Predicting earthquake-induced soil liquefaction based on a hybridization of kernel Fisher discriminant analysis and a least squares support vector machine: a multi-dataset study," *Bulletin of Engineering Geology and the Environment*, vol. 77, no. 1, pp. 191–204, 2018.

[58] Matwork, *Statistics and Machine Learning Toolbox User's Guide*, Matwork Inc., Natick, MA, USA, 2017, https://www.mathworks.com/help/pdf_doc/stats/stats.pdf.

[59] K. De Brabanter, P. Karsmakers, F. Ojeda et al., *LS-SVMlab Toolbox User's Guide Version 1.8*, 2010.